Journal Pre-proof

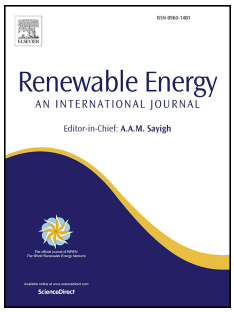

Effect of pretreatment biomass by gas from polyvinyl chloride dehydrochlorination process on maize cob pyrolysis with integrated CO_2 capture

Wojciech Jerzak, Izabela Kalemba-Rec, Aneta Magdziarz

PII: S0960-1481(25)00328-3

DOI: https://doi.org/10.1016/j.renene.2025.122666

Reference: RENE 122666

To appear in: *Renewable Energy*

Received Date: 28 December 2024

Revised Date: 25 January 2025

Accepted Date: 12 February 2025

Please cite this article as: Jerzak W, Kalemba-Rec I, Magdziarz A, Effect of pretreatment biomass by gas from polyvinyl chloride dehydrochlorination process on maize cob pyrolysis with integrated CO_2 capture, *Renewable Energy*, https://doi.org/10.1016/j.renene.2025.122666.

Effect of pretreatment biomass by gas from polyvinyl chloride dehydrochlorination process on maize cob pyrolysis with integrated CO_2 capture

Wojciech Jerzak*, Izabela Kalemba-Rec, Aneta Magdziarz

AGH University of Krakow, Faculty of Metals Engineering and Industrial Computer Science,

Department of Heat Engineering & Environment Protection

Mickiewicza 30, 30-059 Krakow, Poland

*e–mail: wjerzak@agh.edu.pl

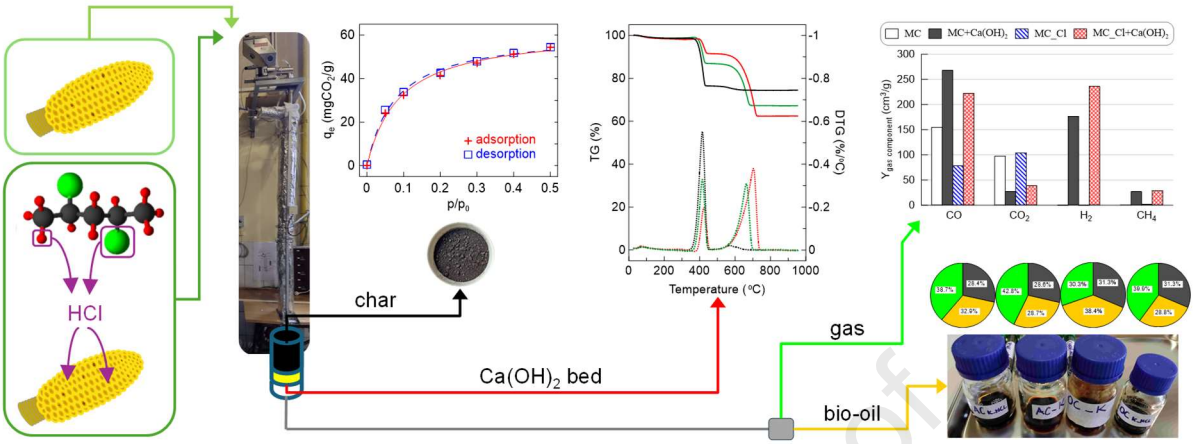

Abstract

This study investigates the effects of pretreatment of maize cob with hydrogen chloride gas obtained from polyvinyl chloride dehydrochlorination on pyrolysis yields and integrated CO_2 capture. The dehydrochlorination process was conducted at 320 °C, while the pyrolysis of the pretreated biomass was performed at 500 °C. Pretreatment significantly altered composition of biomass, reducing hemicellulose from 34.3% to 3.7%, increasing fixed carbon from 15.8% to 20.3%, and increasing the chlorine content from 0.27% to 1.48%. These changes influenced on the thermal decomposition characteristics of maize cob. During fast pyrolysis, the bio–oil yield increased by 17%, from 32.9% to 38.4%, while gas production decreased from 38.7% to 30.3%, indicating a shift towards liquid biofuel production. Integration of calcium hydroxide in the pyrolysis reactor reduced CO_2 emissions by 87%, from 56.5% to 7.5%, and captured chlorine from the pyrolysis gases, minimising harmful residues. Additionally, the use of calcium hydroxide facilitated the generation of hydrogen, increasing its content to 44.7% in the gas phase. The bio–oil produced contained 0.8% chlorine, demonstrating the effectiveness of in–situ chlorine capture. This approach, utilising hydrogen chloride derived from polyvinyl chloride waste, not only reduces environmental impact but also enhances the efficiency and sustainability of bio–oil production.

Keywords: Biomass pretreatment, Fast pyrolysis, PVC dehydrochlorination, Drop–tube reactor, Hydrogen chloride, Calcium hydroxide

1. Introduction

The vulnerabilities of the fossil fuel era and its associated environmental hazards are evident and prompt scientists to look for ways to produce clean energy. According to recent report of the Intergovernmental Panel on Climate Change (IPCC) [1], a profound, rapid, and sustainable reduction in greenhouse gas emissions is necessary. The agreement mandates a reduction in global greenhouse gas emissions by 43% by 2030 relative to 2019 levels, with the ultimate goal of achieving net–zero carbon dioxide emissions by 2050.

Biomass represents a promising alternative to fossil fuels due to its abundance, renewability, and carbon neutrality [2]. Diverse methodologies enable the conversion of biomass into biofuels and biochemicals [3,4]. The most prevalent techniques can be classified as either biochemical or thermochemical. Unlike biochemical conversion, thermochemical pathways can process large amounts of feedstock in relatively short time to produce the desired products and energy [5]. Among the thermochemical conversion processes for biomass, pyrolysis has garnered significant attention due to its focus on producing high–energy–density bio–oil or char, which are advantageous for transportation [6,7]. Over the past decades, biomass pyrolysis has been recognised as one of the most popular and promising methods for producing high–value liquid fuels and chemicals [8]. However, the intricate structure of lignocellulosic biomass poses a formidable challenge because of its resistance to thermal degradation. The structural heterogeneity and resistance of lignin pose challenges to the conversion of cell wall biomass into economically viable products at an industrial scale [9]. Consequently, effective pretreatment strategies are imperative to improve conversion. Various pretreatment techniques have been developed to facilitate the separation of cellulose, hemicellulose, and lignin components in lignocellulosic biomass [10,11]. Figure 1 shows the five basic types of pretreatments of lignocellulosic biomass: physical, biological, physicochemical, chemical, and their combinations. Kumar and Sharma's analysis of pretreatment methods concluded that

pretreatment is a 'tailor–made' process for each specific type of biomass, which requires careful selection and planning based on the unique characteristics of the biomass [11]. So far, no single pretreatment method has been developed that achieves complete delignification of biomass in both an economical and environmentally friendly way. Although combined pretreatment approaches have shown some success, significant research is still required to fully optimise their potential.

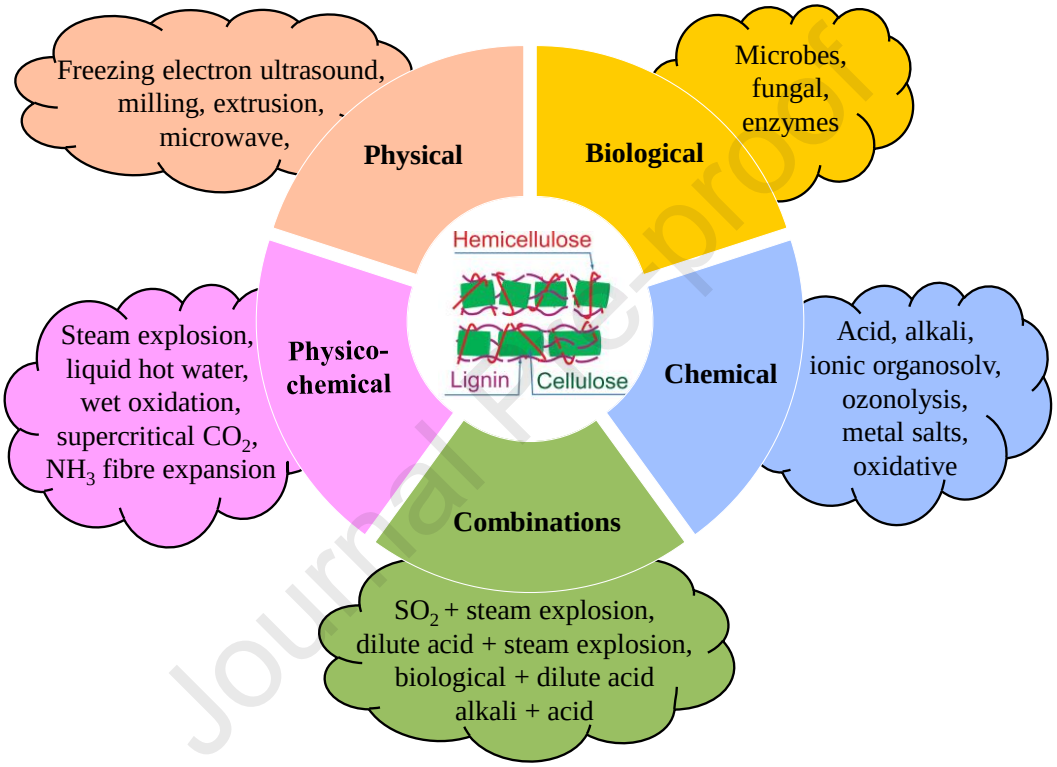

Figure 1. Biomass pretreatment techniques

The significance of pretreatment in the context of lignocellulosic biomass has been well established over time. Through various pretreatment methodologies, reduction in biomass size is achieved, accompanied by the separation of lignin and hemicellulose from the biomass matrix. Moreover, these processes serve to diminish the crystalline structure of cellulose and improve biomass porosity [12].

In recent years, several studies have been carried out on biomass pretreatment using: i) wet acids [13–17], ii) dry acids [18–22], and iii) gaseous acids [23–26]. Acid concentration (in

wet acid pretreatment) significantly influences the efficiency of acid–based biomass pretreatment by promoting diverse structural changes in lignocellulosic biomass through the use of concentrated or dilute acids. After pretreatment, the biomass should be washed with deionised water until the pH value of the filtrate is close to neutral. To reduce wastewater discharge associated with conventional wet acid pretreatment, dry acid pretreatment is proposed, which maintains both the initial feedstock and the final product in the solid state by eliminating the use of water [18]. An alternative method to dry acid pretreatment is the use of acidic gas. The main findings of the literature regarding acid pretreatment of biomass with all methods are summarised in Table 1.

Table 1. Review of the literature on the conditions for acid pretreatment of biomass and the main research findings.

Wet pretreatment conditions			Use of biomass after pretreatment	Main findings	Ref.
Biomass	Acid	Temperature and time			
corn straw	HCl 0.1M [a]	25 °C 4h	feedstock for fast pyrolysis	Biomass pretreatment: i) increased the content of carbon and cellulose while reducing oxygen and effectively removing most metals, especially calcium; ii) decreased the relative content of furans, ketones, phenols, acids,	[13]

				and aldehydes in the bio–oil produced by pyrolysis.	
corn stover	H_2SO_4 0.1M [a]	room temperature 4h	feedstock for fast pyrolysis	The acid washing and the infusion of acid into the biomass were compared. In contrast to acid infusion, acid washing reduced the ash content of the biomass. Pyrolysis of acid–washed biomass promoted levoglucosan production by removing alkali and alkaline earth metals (AAEMs) from the biomass.	[14]
pine sawdust	CH_3COOH 1%, 3% [a]	non–reported 6 h	feedstock for gasification	The acid–sensitive AAEMs present in the biomass would be noticeably depleted, leading to a decrease in catalytic activity in the reactions and,	[15]

				consequently, a reduction in gas production.	
pine wood, straw, bagasse	CH_3COOH 10% [a]	30 °C 10 min	feedstock for fast pyrolysis	The pyrolysis of acid–leached biomass resulted in a reduced char yield and a lower CO_2 content in the pyrolysis gas compared to untreated biomass. The use of pyrolytic acids for biomass pretreatment was most cost–effective when the yield of sugars and bio–oil was 50 t/h.	[16]
palm kernel shell, sawdust	CH_3COOH 5M [a] HCOOH 5M [a] H_2SO_4, 3M, 5M [a] HCl 3M, 5M [a]	room temperature 4 h	feedstock for fast pyrolysis	All acid solutions remove inorganic material, enhancing the production of volatile compounds during pyrolysis. Under the pretreatment conditions analysed, the relative content of ketones and	[17]

				acids decreased. Lignin decomposition was mainly caused by depolymerisation and demethoxylation, forming guaiacol and phenol–type compounds, respectively.	
Dry pretreatment					
corn stover	H_2SO_4 25 mg/g [b]	185 °C 3 min	feedstock for hydrolysis	The pretreatment of the biomass most favoured the formation of glucose and xylose. Up to 80% ethanol can be obtained from biomass after pretreatment.	[19]
corn stover	H_2SO_4 25 mg/g, 50 mg/g [b]	175 °C 90 min	–	This method reduced corrosion problems by approximately 85% and paved the way for large–scale application.	[20]
sunflower, artichoke,	H_2SO_4 25 mg/g,	175 °C, 185 °C	feedstock for biodetoxification	The efficiency of pretreatment was	[21]

and stevia stalks	50 mg/g [b]	5 – 15 min		mainly influenced by concentration of H_2SO_4. The reduction in the solid–liquid ratio (2:1 to 0.5:1) increased degradation products, while increasing the temperature (175 °C to 185 °C) significantly reduced the xylan content and increased inhibitor formation.	
wheat straw	H_2SO_4 10 – 25 mg/g [b]	175 – 185 °C 3 min	feedstock for hydrolysis	It was shown that 66% of the carbon from lignocellulose was recovered as ethanol, xylose, and reactive lignin.	[22]
Pretreatment with acid gases					
corn starch	HCl	25–45 °C 1–8 h	–	As the degradation time and temperature increased, the molecular weight of starch gradually	[23]

				decreased, and the range of gelatinization temperatures widened.	
scots pine	HCl	room temperature, 2, 6 and 18 h	–	The initial moisture content of biomass before HCl treatment had a more significant impact on hydrolysis than the duration of exposure to the acidic gas. In particular, a higher initial moisture content was associated with increased hemicellulose degradation.	[24]
aspen wood, flour	HCl	room temperature 0.5–24 h	–	Biomass samples were effectively hydrolysed using HCl gas, allowing the selective and efficient removal of C5 sugars. The optimal conditions were determined to be a 60–40% moisture	[25]

				content and a 6–hour reaction time, achieving a recovery of 84% of the available xylan from the biomass.	
birch pulp	HCl	room temperature 1–335 h	–	HCl can effectively degrade cellulose into glucose when the moisture content of the cellulosic fibres is maintained at 50%. Additionally, the introduction of chlorite into the system prevents the formation of harmful humins.	[26]

[a] – concentration of acid in solution, [b]acid usage – expressed as the mass of acid per mass of dry mass.

The primary objective of this research is to investigate the impact of pretreatment of maize cob biomass with hydrogen chloride (HCl) derived from the dehydrochlorination of polyvinyl chloride (PVC), on the yields of the pyrolysis product and the integration of CO_2 capture during the process. This study aims to: (i) Evaluate the chemical and structural modifications induced in biomass through gaseous HCl pretreatment, (ii) Examine the effects of these modifications on pyrolysis efficiency, including the distribution of bio–oil, gas, and

char yields, (iii) Assess the role of calcium hydroxide ($Ca(OH)_2$) in capturing chlorine and CO_2 during pyrolysis to improve environmental sustainability, and (iv) Identify potential applications of pyrolysis products in biofuels and material science.

This study introduces a new approach to biomass pretreatment and pyrolysis by using hydrogen chloride gas derived from the dehydrochlorination of polyvinyl chloride (PVC) waste. This method offers dual benefits: it valorises PVC waste and enhances biofuel production. The research highlights significant advancements in three key areas: i) the pretreatment process for biomass, which improves thermal decomposition characteristics; ii) the enhancement of bio-oil yield and quality, indicating the potential for efficient liquid biofuel production; and iii) the integration of CO_2 through the application of calcium hydroxide in the pyrolysis reactor, which enables the production of hydrogen-rich gas. This innovative combination of PVC waste-derived HCl pretreatment, sustainable bio-oil production, and integrated pollutant mitigation provides a new solution for biomass conversion that aligns with sustainable waste management practices.

2. Materials and methods

2.1. Materials

The maize cob (MC) from a farm located in Lesser Poland constituted the basic research feedstock. Preparing processes included grinding maize cobs and sieving to obtain a repeatable drying fraction of approximately 3 mm in diameter. The prepared ground maize cob, hereinafter referred to as MC, was the first batch of material for pyrolysis. The second batch of material was maize cob pretreatment with hydrogen chloride (named MC_Cl) from the low temperature dehydrochlorination process of polyvinyl chloride (PVC). The PVC powder was purchased from Sigma–Aldrich (No. 81388). The additional material used for the pyrolysis of MC and MC_Cl was calcium hydroxide purchased from Chempur (1305–62–0) with a purity of min. 95% $Ca(OH)_2$ and max. 4% $CaCO_3$. The basic criterion for the selection of calcium hydroxide

was the economic aspect. Calcium hydroxide is almost twice cheaper than calcium oxide, which justifies the choice of this material. As a result, costs are reduced by building a larger scale of the process. At the same time, as recently reported by Dostie et al. [27], calcium oxide in contact with humid air is easily covered with a thin film of water, which favours the formation of calcium hydroxide. Moreover, in contact with air, it captures CO_2 to form $CaCO_3$. The increased changes in the composition of CaO make the use of pure CaO for the pyrolysis process extremely difficult and require the establishment of appropriate conditions.

2.2. Research methods

2.2.1. Pretreatment and pyrolysis

Maize cob (MC) pretreatment consisted of rinsing the biomass with gas from the PVC dehydrochlorination process, as shown in Fig. 2a). The most important parameters of the dehydrochlorination process are listed in Table 2. A glass bottle containing 200 g of MC was blown with gas resulting from the dehydrochlorination PVC. The temperature of the PVC dehydrochlorination process (320 ^{o}C) and the composition of the resulting gas were previously determined on the basis of thermogravimetry–Fourier transform infrared spectroscopy tests, in previous work [28]. The dominant pyrolysis product was hydrogen chloride (HCl) diluted with a nitrogen flow of 100 ml/min. Biomass pretreatment was carried out at a temperature of 25 ^{o}C. After the pretreatment time of MC with hydrogen chloride was completed, the MC_Cl was poured into the microfeeder of the pyrolysis reactor. The mechanism of HCl removal from PVC has been extensively investigated in the literature [29,30], involving successive steps such as dehydrochlorination with the formation of conjugated double bonds, polymer chain scission, and the formation of organic compounds from the fragmented chains. The HCl gas was absorbed by the water (i.e. moisture) present on the MC surface and led to a hydrolysis reaction.

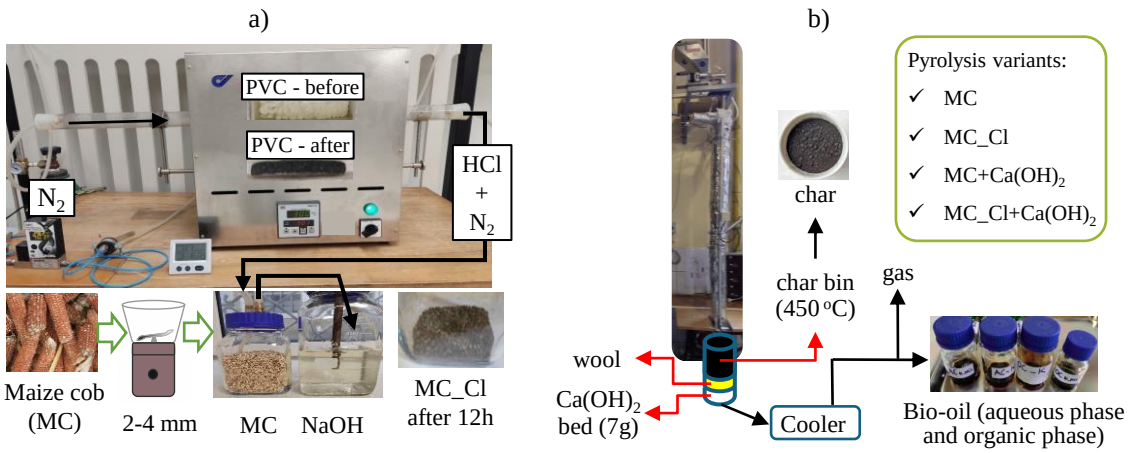

127

128 Figure 2. Photographs featuring descriptive elements illustrating the experimental procedures:
129 a) dehydrochlorination of PVC and b) pyrolysis of maize cob for the variants analysed

130 The pyrolysis process was carried out in a drop–tube reactor at 500 °C, with a biomass
131 feed rate of 1.76 g/min (see Table 2). A nitrogen atmosphere with a flow rate of 1 l/min provided
132 a residence time of the vapour of 34 s. The lower section of the reactor contained a char bin and
133 a calcium hydroxide ($Ca(OH)_2$) bed to capture chlorine from the hot pyrolysis gases. The
134 temperature in the $Ca(OH)_2$ bed was kept at 450 °C, with 7.0 g of $Ca(OH)_2$ in the bed. After the
135 bio–oil was condensed, the cooled pyrolysis gas was collected in a Tedlar bag for composition
136 analysis.

137 Table 2. The most important parameters of the PVC dehydrochlorination process and maize
138 cob pyrolysis.

Process parameters	Value
Dehydrochlorination	
Nitrogen flow (ml/min)	100
Temperature (°C)	320
Residence time at 320 °C (min)	40
Mass of sample (g)	2

Number of PVC samples (–)	18
Pyrolysis	
Nitrogen flow (l/min)	1
Temperature (°C)	500
Vapour residence time (s)	34
Feeding rate (g/min)	1.76
Heating rate (°C/s)	500

2.2.2. Proximate, ultimate and fibre analysis

The parameters included in the proximate analysis, i.e. moisture, volatile matter, and ash content, were determined in accordance with the standards ISO 18134 [31], ISO 18123 [32] and ISO 18122 [33], respectively. Fixed carbon was calculated as a difference.

The ultimate analysis of biomass, char and bio–oil including carbon, hydrogen and nitrogen content was determined using a Truspec CHNS 628 Leco analyser, according to ISO 16948 [34]. The chlorine content was determined on the basis of ISO 587 [35]. Oxygen was calculated as the difference.

Biomass fibre analysis was performed, based on the van Soest method, to determine acid detergent fibre, acid detergent lignin, and neutral detergent fibre. The analyses were carried out on the basis of ISO 16472 [36] and ISO 13906 [37]. All analyses were repeated at least twice.

2.2.3. Fourier transform infrared spectroscopy

The Fourier transform infrared spectroscopy technique was used to identify the functional groups of organic compounds present in the studied maize cobs and their derived chars. The analyses were performed using a Bruker Alpha II spectrometer, covering the infrared absorption range of 400 to 4000 cm^{-1}.

2.2.4. Gas analysis

The composition of pyrolytic gas was analysed using an Agilent Technologies 7890A gas chromatograph equipped with a thermal conductivity detector and a flame ionisation detector. Helium was used as the carrier gas at a flow rate of 30 ml/min. This setup allowed the detection of CH_4, H_2, O_2, N_2, CO, CO_2, and hydrocarbons (C_xH_y). Each sample was analysed at least twice to ensure repeatability of the result.

2.2.5. Scanning electron microscopy

The morphology of the biomass and chars was examined by Inspect S50 scanning electron microscopy. The biomass and char particles studied were mounted on metal stubs using double–sided carbon adhesive discs. The samples were observed in low–vacuum mode by secondary electrons using a large–field–detector detector. The applied accelerating voltage was 12.5 kV.

2.2.6. Thermal analysis

The thermal analysis of the sorbent, i.e. $Ca(OH)_2$ was performed using a Mettler Toledo TGA/DSC Star System analyzer. The sample masses were approximately 5 mg. The analyses were carried out in air atmosphere (40 ml/min) at temperatures ranging from 25 °C to 950 °C in sapphire crucibles.

2.2.7. Carbon dioxide adsorption of char

The CO_2 sorption–desorption experiments were conducted using a gravimetric sorption analyzer (IGA–001, Hiden Isochema, UK). Approximately 0.4 g of the sample were dried at 105 °C for 12 hours before analysis. Before sorption measurement, the sample was subjected to a degassing process for 12 hours using a turbomolecular pump to ensure the removal of adsorbed gases or moisture. To determine the sorption capacity for CO_2, the temporal changes in the weight of the sample were monitored until stabilisation (i.e. no significant weight increase was observed). Sorption isotherms were obtained by repeating the gas dosing procedure

multiple times and waiting for equilibrium stabilisation at various CO_2 pressures (0.05, 0.1, 0.2, 0.3, 0.4, and 0.5 MPa). The desorption process was initiated by stepwise depressurisation of CO_2 within the reactor chamber, during which the weight loss of the sample was recorded until stabilisation. The stabilisation point indicated the complete release of the adsorbed gas.

The Langmuir isotherm model was used to describe the sorption of carbon dioxide on the tested chars in the form [38]:

$$q_e = \frac{q_m \cdot K_L \cdot p}{1 + K_L \cdot p} \quad (1)$$

where:

q_e – equilibrium adsorption at pressure p, mg CO_2/g,

p – equilibrium pressure, Pa,

q_m – maximum sorption capacity of the char at 25 °C with p approaching ∞, mg CO_2/g,

K_L – Langmuir constant, Pa.

2.2.8. Specific surface area

The textural properties of the sorbents were characterised by nitrogen adsorption measurements performed at −195.8 °C using a Micromeritics ASAP 2020 Plus analyzer. The nitrogen adsorption isotherms were utilised to determine the Brunauer–Emmett–Teller specific surface area.

3. Results

3.1. Effect of pretreatment on biomass and char

3.1.1. Proximate, ultimate, and fibre analyses of maize cob

The results of the proximate, ultimate, and fibre analyses for MC and MC_Cl are shown in Table 3. Moisture, ash, and fixed carbon contents increased in MC_Cl. Pretreatment of the maize cob with hydrogen chloride (MC_Cl) promoted the formation of H_2O by reactions (2) and (3) with functional groups containing oxygen (such as hydroxyl and carboxyl groups) in biomass:

$$R - OH + HCl \rightarrow R - Cl + H_2O \quad (2)$$

$$R - COOH + HCl \rightarrow R - COCl + H_2O \quad (3)$$

where:

R – any organic fragment in which a carbon atom is directly bonded to a functional group.

As a result, the moisture content of MC_Cl was two times higher than that of MC. The observed upward trend is due to the use of a gaseous form of acid. The opposite trend of changes was reported when biomass was washed with acids, during which, among other things, inorganic elements were washed [13–15]. In interpreting the results of the ultimate analysis, the effect of acid pretreatment on carbon content was negligible. The expected result of the biomass pretreatment with hydrogen chloride was a slight increase in hydrogen and a significant increase in chlorine. The chlorine content in MC_Cl was 0.27%, while after 12 hours of pretreatment with hydrogen chloride it increased to 1.48%. In terms of interpreting the fibre results, the significant reduction in the cellulose content was observed suggesting that the pretreatment with hydrogen chloride effectively breaks down structure of cellulose. Cellulose depolymerization occurs by breaking glycosidic bonds to release glucose [39]. The evident decrease (from 34.3% to 3.7%) in hemicellulose indicates that hemicellulose is highly susceptible to acid pretreatment [40]. Lignin is more resistant to acid hydrolysis tend to increase in relative content.

Table 3. Proximate, ultimate, and fibre analysis of raw maize cob (MC) and maize pretreatment with hydrogen chloride (MC_Cl)

Proximate analysis [a] (%)	MC	MC_Cl
Moisture, M	8.35	17.46
Volatile matter, VM	74.35	59.98
Ash, A	1.46	2.22
Fixed carbon, FC	15.84	20.34

Ultimate analysis [a] (%)		
Carbon, C	43.94	43.67
Hydrogen, H	6.15	6.32
Nitrogen, N	0.35	0.27
Chlorine, Cl	0.27	1.48
Oxygen, O	47.83	46.04
Fibre analysis [a] (%)		
Cellulose	45.32	34.69
Hemicellulose	34.31	3.71
Lignin	4.14	11.27
Extractives	14.77	48.11

[a]ad: air–dried basis.

3.1.2. Fourier transform infrared spectroscopy

The presence of functional groups in the pyrolysis feedstocks (MC, MC_Cl) and products (char, and char_Cl) was analysed using Fourier transform infrared spectroscopy (FTIR). Figure 3 shows the effect of pretreatment with hydrogen chloride of MC on peak FTIR spectra. When comparing the spectra for the MC and MC_Cl samples, the noteworthy peaks are marked with dashed lines in Figure 2. The spectra of the MC and MC_Cl samples are similar, and no new functional groups were formed in the MC_Cl sample. The peaks at 3327 and 3282 cm^{-1} correspond to stretching vibrations of O–H, indicating the presence of hydroxyl groups of cellulose and hemicellulose [13]. The peaks are slightly less intense in MC_Cl, suggesting a minor reduction in the hydroxyl content due to hydrogen chloride pretreatment. The absorption at 2918 and 2854 cm^{-1} represent the stretching of $–CH_3$ and $–CH_2$ [41]. The

peaks are slightly less intense in MC_Cl, suggesting a minor reduction in the hydroxyl content due to hydrogen chloride pretreatment.

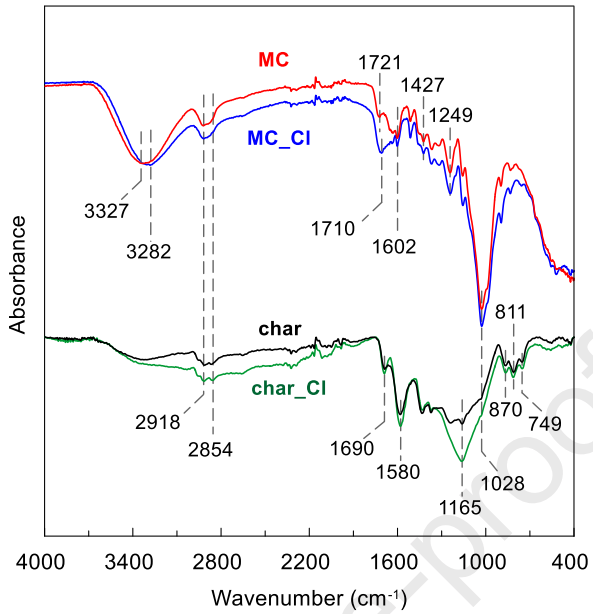

Figure 3. FTIR spectra of feedstocks and chars

A slight shift in wavenumber is also observed in the C=O peaks stretching vibrations from carbonyl groups, due to pretreatment of the MC sample with hydrogen chloride [42]. This suggests the degradation of hemicellulose as a result of hydrogen chloride pretreatment. In both feedstocks, the peaks responsible for aromatic compounds (C=C at 1602 cm^{-1}) and carbohydrates (C–H bending at 1427 cm^{-1}) and (C–O stretching vibrations at 1249 cm^{-1}) are identified. The last peak that is most intense corresponds to the stretching of C–O (1028 cm^{-1}) in polysaccharides [17]. The breakdown of these structures during pyrolysis confirmed the flattening of the char and char_Cl spectrum. In turn, peaks 870, 811, and 749 cm^{-1} can represent both aromatic compounds in char and char_Cl such as bending out–of–plane C–H and stretching C–Cl. Enhanced formation of carbonyl and aromatic structures in char_Cl, suggests that hydrogen chloride pretreatment before pyrolysis facilitates the production of these compounds. In the char_Cl sample, two bands at 1580 cm^{-1} (C=C stretching) and 1165 cm^{-1}

(C–O stretching) are characterised by significantly higher intensity compared to the char sample. These are characteristic peaks for lignin [43].

3.1.3. Scanning electron microscopy

Figure 4 shows scanning electron microscopy (SEM) micrographs of biomass (MC and MC_Cl), its chars and calcium hydroxide $Ca(OH)_2$ – before pyrolysis, $Ca(OH)_2$-MC – after pyrolysis MC, and $Ca(OH)_2$-MC_Cl – after pyrolysis MC_Cl. The MC particles are dense with less developed surface compared to the MC_Cl particles. The pretreatment of the MC with hydrogen chloride evidently increased the porosity of the MC_Cl particles. The pyrolysis process causes damage to the structure of the biomass. The chars are characterised by typical 3–dimensional char structure. Both chars exhibited the tubular–shaped structure with micropores. The effect of chlorine is observed on the surface of char_Cl. Chlorine caused the more degraded structure of char_Cl. The SEM examination had proved that the $Ca(OH)_2$ particles before the pyrolysis process had irregular (agglomerated) shapes. The surface of $Ca(OH)_2$ particles was frayed. The $Ca(OH)_2$ particles exhibit high surface roughness. The particles of $Ca(OH)_2$-MC and $Ca(OH)_2$-MC_Cl are more solid, but the surface is also rugged. The particle size of $Ca(OH)_2$-MC_Cl is smaller than that of the $Ca(OH)_2$-MC particles. Finer particles can be described as the reaction of $Ca(OH)_2$ with chlorine and CO_2. The $Ca(OH)_2$ bed has a catalytic effect on the pyrolysis gas leaving the reactor, leading to its coking.

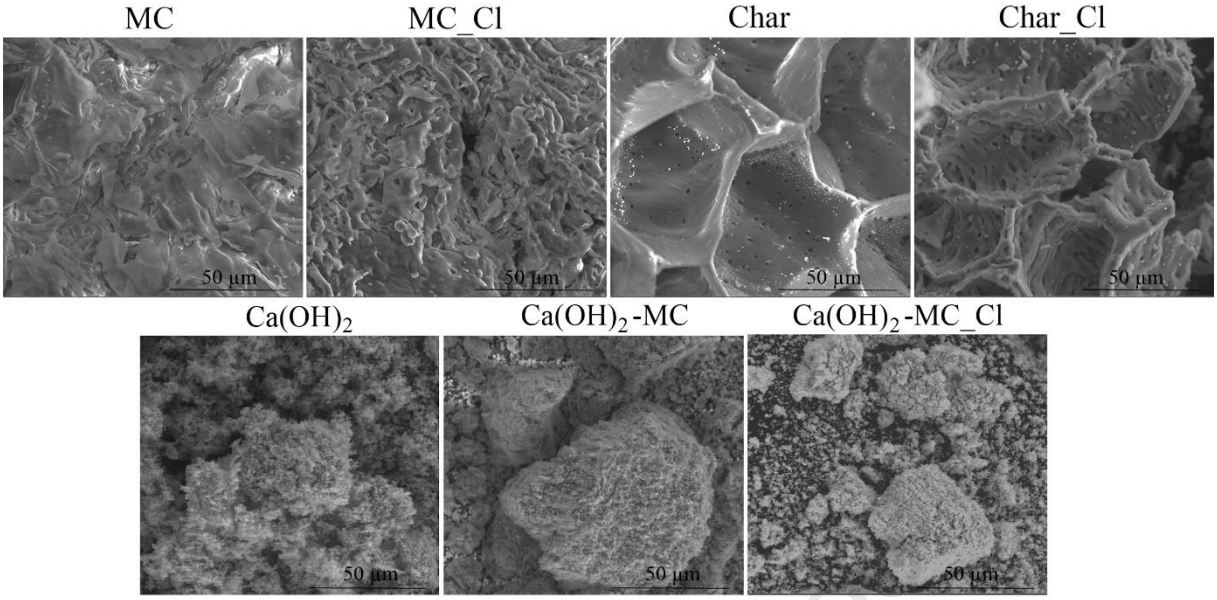

Figure 4. SEM micrographs of feedstocks, chars, and calcium hydroxide

3.1.4. Carbon dioxide adsorption on char

To evaluate the potential application of chars, carbon dioxide (CO_2) sorption capacity experiments were conducted. Figures 5a and 5b present adsorption and desorption isotherms of CO_2 on char and char_Cl samples, respectively. The adsorption capacity, q_e (mg CO_2/g sample), is shown as a function of relative pressure (p/p_0). The experimental data were fitted to the Langmuir isotherm model, and the Langmuir constants are provided in the legend. The Langmuir model assumes the occurrence of an energetically homogeneous surface, i.e. identical sorption centres. The quality of the fit of mathematical models to the data obtained from the sorption experiments was analysed. For the char sample (Fig. 5a), the adsorption and desorption isotherms are well described by the Langmuir model, as indicated by the high determination coefficients ($R^2 > 0.9959$). In particular, the K_L parameter for desorption (1.277) is higher than for adsorption (1.121), suggesting differences in the binding mechanisms of CO_2 during the adsorption and desorption processes. A similar trend is observed for the char_Cl sample (Fig. 5b), with the model also exhibiting a high degree of fit ($R^2 > 0.9966$). Here, the K_L parameter

for desorption (1.168) exceeds that for adsorption (1.078), indicating comparable adsorption–desorption characteristics to the char sample.

However, the CO_2 adsorption capacity of the char_Cl sample is slightly lower compared to the char sample. At a pressure of 0.1 MPa (25 °C) the adsorption of CO_2 on char was 32.4 mg CO_2/g while on char_Cl it was 31.2 mg CO_2/g. This reduced adsorption capacity may result from changes in microporosity or the creation of less favourable adsorption sites due to structural modifications that could limit the materials ability to retain CO_2 molecules effectively. A similar result (33 mg CO_2/g) was reported for unmodified chars derived from corn kernel [44].

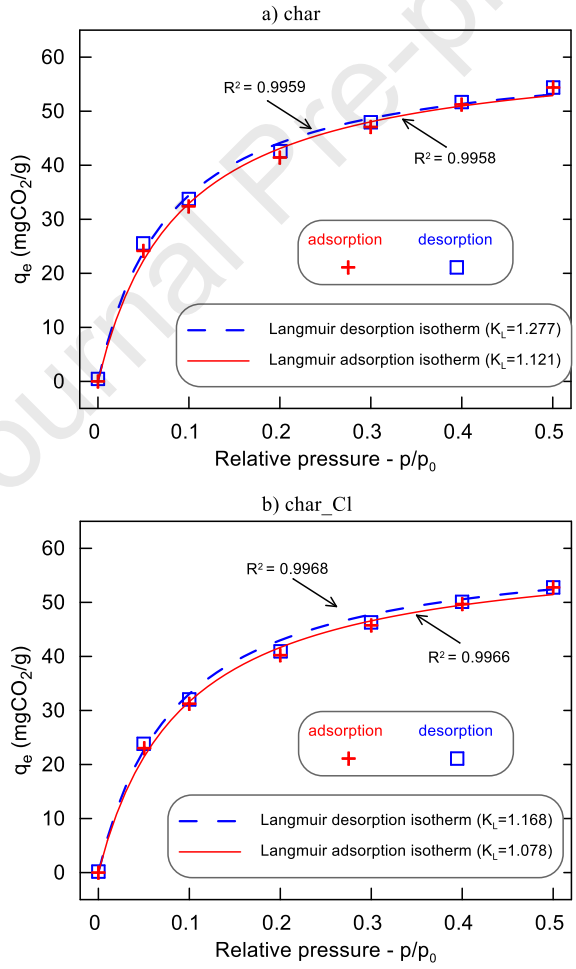

Figure 5. Carbon dioxide adsorption/desorption Langmuir isotherms chars from a) MC and b) MC_Cl samples

3.2. Characteristics of pyrolysis process

3.2.1. Yield of pyrolysis

Figures 6a – d) illustrate the yields of gas, bio–oil and char from the pyrolysis of: a) untreated maize cob (MC), b) untreated maize cob (MC+$Ca(OH)_2$) with the flow of hot pyrolytic vapours through the $Ca(OH)_2$ bed, c) pretreatment of the maize cob with hydrogen chloride (MC_Cl) and d) pretreatment of the maize cob with hydrogen chloride followed by the use of $Ca(OH)_2$ to capture chlorine gas (MC_Cl+$Ca(OH)_2$). The pretreatment of MC with hydrogen chloride significantly alters the yield distribution of the pyrolysis products. There is a notable reduction in the gas yield from 38.7% (for MC pyrolysis) to 30.3% (for MC_Cl pyrolysis). This decrease indicates that acid pretreatment likely influences the decomposition pathways of the biomass, reducing the formation of gaseous products. The bio–oil yield increases substantially from 32.9% (for MC pyrolysis) to 38.4% (for MC_Cl pyrolysis), suggesting that hydrogen chloride pretreatment enhances the conversion of biomass into liquid products. Char yield shows a slight increase from 28.4% (Fig. 6a) to 31.3% (Fig. 6c). The pyrolysis of MC_Cl significantly enhances the bio–oil yield while reducing the gas yield. However, when $Ca(OH)_2$ is added to the pyrolysis system, the gas yield increases again, suggesting a trade–off between gas and bio–oil production, depending on the pretreatment used. The char yield remains relatively stable across in pretreatments. These findings highlight the importance of pretreatment methods in optimising the yield of the desired pyrolysis products and suggest that the combination of chemical pretreatments can effectively modulate the distribution of the pyrolysis products. The application of $Ca(OH)_2$ to MC_Cl pyrolysis increases the gas yield from 30.3% to 39.9%. This suggests that $Ca(OH)_2$, possibly through its role in chlorine capture, facilitates the breakdown of biomass into gaseous products, reversing some of the effects of hydrogen chloride pretreatment. Bio–oil yield decreases from 38.4% to 28.8% with the addition of $Ca(OH)_2$. This reduction implies that while $Ca(OH)_2$ may help capture

chlorine and mitigate its adverse effects, it also shifts the balance toward increased gas production at the expense of bio–oil yield. The char yield remains constant at 31.3% after the addition of $Ca(OH)_2$, indicating that the formation of solid residues is not significantly affected by the presence of $Ca(OH)_2$ in the system. Overall, the main advantages of $Ca(OH)_2$ used in MC pyrolysis are non–toxicity and low cost.

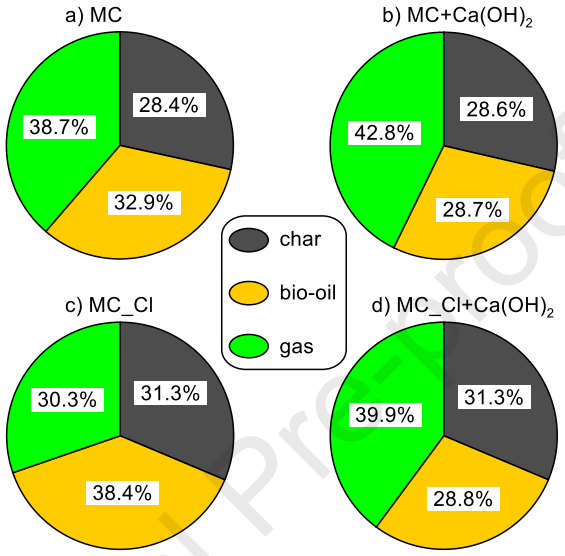

Figure 6. Yields of products from pyrolysis: a) MC, b) MC+ $Ca(OH)_2$, c) MC_Cl and d) MC_Cl+ $Ca(OH)_2$

3.2.2. Composition of pyrolysis products – condensed phase and calcium hydroxide

Figure 7 shows the composition of the products from pyrolysis MC and MC_Cl that reveals key insights into their potential applications. Bio–oil included two phases: organic condensed (OC) and aqueous condensed (AC), which were separated by gravity separation. Char from MC pyrolysis exhibits a high carbon content at 72.4%, typical of biochar, which makes it suitable for soil amendment and carbon sequestration [45]. Importantly, the chlorine content of char (0.3%) and char_Cl (1.5%) does not prevent its use as a soil amendment. Chlorine, in small amounts, is a micronutrient for plants and could provide this essential nutrient. Additionally, the presence of chlorine can help to alter soil pH [46]. The carbon content

of char_Cl increases to 76.7%, suggesting an enhancement in the fixed carbon fraction due to the pretreatment with hydrogen chloride of MC. The chars have a relatively low hydrogen content (4.8 and 3.7%), while OC, OC_Cl, AC and AC_Cl have higher hydrogen contents (7.7, 9.4, 7.1, and 8.5%, respectively), reflecting more hydrogen–rich organic compounds and water. On the basis of the carbon and hydrogen content, OC is more attractive for future applications. The OC and AC phases have lower carbon contents at 53.9% and 24.4%, respectively. Chlorine in the maize cob matrix can lead to the formation of organochlorine compounds. These compounds can retain oxygen in the bio–oil (OC_Cl and AC_Cl) instead of releasing it as CO in the gas phase. Despite the use of a $Ca(OH)_2$ bed, the OC and OC_Cl fraction contained 0.07% and 0.8% chlorine, respectively. OC_Cl containing 0.8% chlorine can have potential applications in several areas where the low chlorine content is manageable and does not pose significant risks. OC and OC_Cl can serve as feedstocks to produce valuable chemicals, such as phenols, furans, and other bio–based chemicals [47]. OC and OC_Cl can also be used in the production of adhesives, binders, and resins [48].

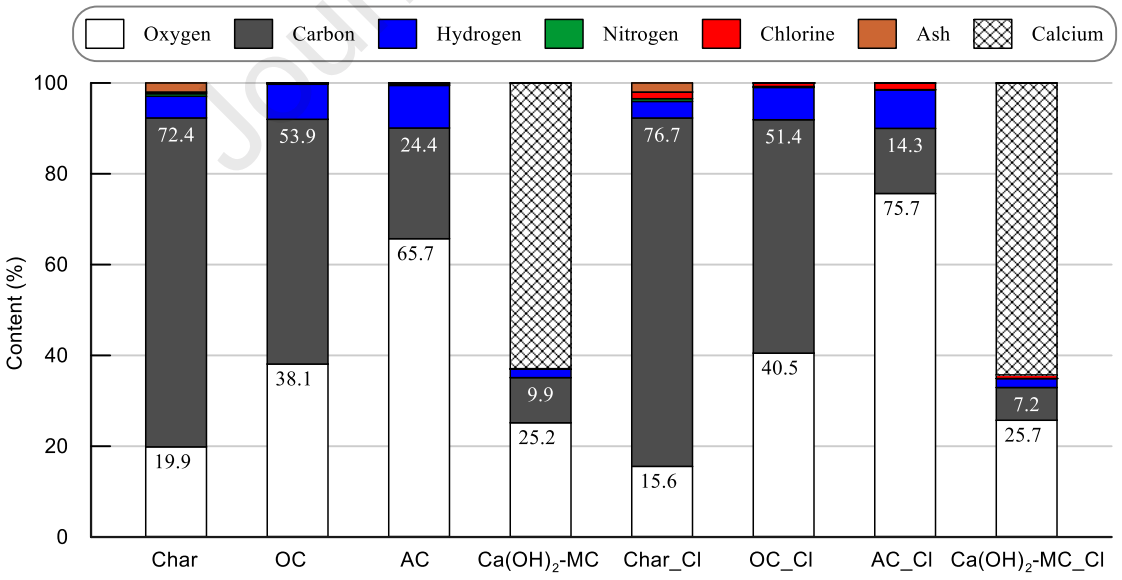

Figure 7. Composition of condensed pyrolysis products and calcium hydroxide

The low chlorine content ensures that the final products are free of harmful and corrosive

properties, making them suitable for various industrial applications. $Ca(OH)_2$ coked relatively quickly. The results presented in Fig. 7 show the analyses for $Ca(OH)_2$-MC and $Ca(OH)_2$-MC_Cl performed after 4 minutes of the pyrolysis process. In particular, $Ca(OH)_2$-MC had a lower carbon content (7.2%) than $Ca(OH)_2$-MC_Cl (9.9%). The progress of coke formation on the $Ca(OH)_2$-MC_Cl surface was influenced by the chlorine content in the gas. The pyrolysis gas of the MC_Cl sample contained more chlorine than the pyrolysis gas of the MC sample. Chlorine reacted with $Ca(OH)_2$ to form calcium chloride, changing the reactivity of $Ca(OH)_2$, which was less susceptible to coking. Notably, the retention of chlorine in $Ca(OH)_2$ allowed for the reduction of the acidity of the pyrolysis gas. The detailed distribution of chlorine into pyrolysis products and calcium hydroxide is shown in Fig. 1S (supplementary materials).

3.2.3. Composition and yield of pyrolysis gas

Table 4 provides a nitrogen–free composition of gas obtained from the pyrolysis of: MC, MC+$Ca(OH)_2$ (MC with a $Ca(OH)_2$ bed), MC_Cl, and MC_Cl+ $Ca(OH)_2$. As part of the analysis, the percentage contents of CO, CO_2, H_2, CH_4 and other hydrocarbons (C_xH_y) were measured in the pyrolysis gas. Two main components, CO (61%) and CO_2 (38.4%), were revealed in the pyrolysis gas of MC. At the same time, this gas was the richest in CO among the pyrolysis variants considered. The CO_2 content was highest for the MC_Cl pyrolysis, indicating that hydrogen chloride pretreatment promotes CO_2 formation. However, the addition of $Ca(OH)_2$ significantly reduces the CO_2 content in both MC and MC_Cl cases, suggesting that $Ca(OH)_2$ absorbs CO_2 [49]. The use of a $Ca(OH)_2$ bed, that is, pyrolysis of the MC+ $Ca(OH)_2$ sample promoted the formation of H_2 up to 35.2%, 5.4% CH_4 and reduced the CO_2 content to 5.5%, compared to MC pyrolysis. With respect to samples pretreated with hydrogen chloride (MC_Cl and MC_Cl+$Ca(OH)_2$), the CO_2 reduction result obtained should be considered satisfactory, because the change from 56.5% to 7.5% means a reduction in CO_2 of 87%. The results also show that H_2 is present only when $Ca(OH)_2$ is used, with the highest

content during the pyrolysis of MC_Cl+$Ca(OH)_2$ samples. This indicates that $Ca(OH)_2$ significantly promotes H_2 production, especially when combined with pretreatment with hydrogen chloride, suggesting a synergistic effect. Similar conclusions can be drawn for CH_4, which means that $Ca(OH)_2$ improves CH_4 formation during pyrolysis. The C_xH_y content (mainly ethylene and ethane) in the pyrolysis gas remained very low for the samples analysed, ranging from 0.1% to 0.5%. On the basis of the content of each gas components, the higher heating value (HHV) of the pyrolysis gas was calculated from Eq. (4).

$$HHV_{gas} = \frac{CO \cdot 12.63 + H_2 \cdot 12.48 + CH_4 \cdot 39.82 + C_2H_4 \cdot 63.41}{100\%} \quad (4)$$

where:

CO, H_2, CH_4, C_2H_4 – percentages of pyrolysis gas components (%) from Table 2.

Ethylene (C_2H_4), the main component of hydrocarbons, has been used to calculate the HHV of C_xH_y. As shown in Table 4, the highest HHV were obtained when hot pyrolytic gases flowed through the $Ca(OH)_2$ bed. It was 13.6 MJ/m^3 and 13.3 MJ/m^3 for the MC+ $Ca(OH)_2$ and MC_Cl+ $Ca(OH)_2$ samples, respectively. This confirms the catalytic effect of $Ca(OH)_2$. The HHV of gas without flow through the $Ca(OH)_2$ bed was much lower and amounted to 7.9 MJ/m^3 for MC and 5.8 MJ/m^3 for MC_Cl.

To look more objectively at the gases produced during pyrolysis, their yields were expressed in cm^3 per gramme of feedstock. For this purpose, the following were calculated: density under standard conditions (d_{gas}) using Eq. (5); gas volume flow ($\dot{V}_{gas}$) using Eq. (6), and finally the yield of individual gas components ($Y_{CO}, Y_{CO_2}, Y_{H_2}, Y_{CH_4}, Y_{C_xH_y}$) from Eq. (7).

$$d_{gas} = \frac{CO \cdot d_{CO} + CO_2 \cdot d_{CO_2} + H_2 \cdot d_{H_2} + CH_4 \cdot d_{CH_4} + C_2H_4 \cdot d_{C_2H_4}}{100\%} \quad (5)$$

$$\dot{V}_{gas} = \frac{\dot{m}_{gas}}{d_{gas}} \quad (6)$$

$$Y_{CO} = \frac{CO \cdot \dot{V}_{gas}}{100\%} \quad (7)$$

where:

d_{CO} – density (g/cm^3) of CO under standard conditions,

$\dot{m}_{gas}$ – gas mass yield (g gas/g feedstock) from Figure 6,

CO – percentages of CO (vol. %) from Table 3.

Table 4. Composition of pyrolysis gas and corresponding HHV

Gas component	MC	MC+Ca(OH)$_2$	MC_Cl	MC_Cl+Ca(OH)$_2$
CO (%)	61.0	53.4	42.6	42.1
CO_2 (%)	38.4	5.5	56.5	7.5
H_2 (%)	0	35.2	0	44.7
CH_4 (%)	0	5.4	0.8	5.5
C_xH_y (%)	0.1	0.5	0.12	0.3
HHV (MJ/m^3)	7.9	13.6	5.8	13.3

The yields of gas components determined on the basis of Eq. (7) are shown in Fig. 8. The use of a Ca(OH)$_2$ bed evidently promoted the production of CO, H_2, CH_4 and C_xH_y. CO formation increased from 155 cm^3/g to 268 cm^3/g when MC was used as the feedstock, and from 78 cm^3/g to 222 cm^3/g when MC_Cl sample was used. Pretreatment with maize cob with hydrogen chloride changes the paths of thermal decomposition of biomass. The CO yield from MC_Cl was half that of MC. This may suggest suppression of the decarbonylation reaction (8).

$$R - CHO \rightarrow R - H + CO \quad (8)$$

The presence of chlorine can change the catalytic properties of inorganic compounds in MC_Cl (such as alkali metals and alkaline earth metals), leading to different pyrolysis pathways. Chlorine might facilitate the formation of more stable oxygenated compounds rather than gaseous CO. Additionally, biomass pretreatment significantly enhanced hydrogen (H_2) production. The hydrogen yield increased from 177 cm³/g for MC+Ca(OH)$_2$ to 236 cm³/g for MC_Cl+Ca(OH)$_2$. For comparison, previous studies under similar temperature conditions

(550 °C) reported the following results: Magoua Mbeugang et al. [50] achieved a hydrogen yield of 189.88 cm^3/g from cellulose in the presence CaO, while Tang et al. [51] reported 0.57 mmol/g from the co-pyrolysis of biomass and plastics in the presence of CaO.

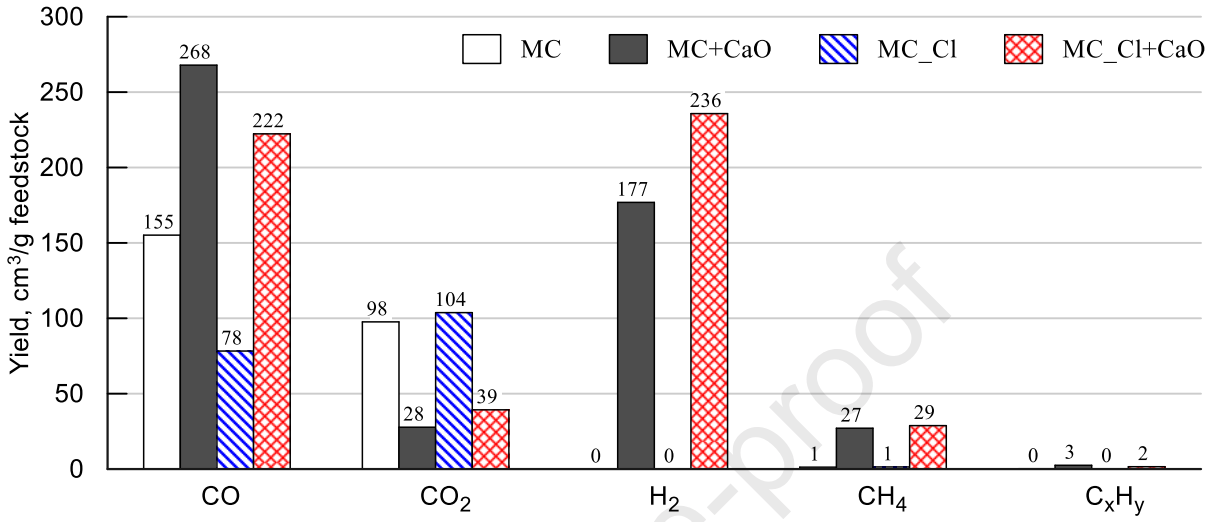

Figure 8. Yield of pyrolysis gases for studied samples

3.3. Analysis of calcium hydroxide

Thermal analysis (TG and DTG) was conducted for three samples: $Ca(OH)_2$, $Ca(OH)_2$ exposed to pyrolysis gases from maize cob ($Ca(OH)_2$-MC), and $Ca(OH)_2$ exposed to pyrolysis gases from maize cob after pretreatment with HCl ($Ca(OH)_2$-MC_Cl) and they are shown in Figure 9. The first major peak at ~415 °C, observed in all samples, corresponds to the dehydroxylation of $Ca(OH)_2$ according to the reaction:

$$Ca(OH)_2 \rightarrow CaO + H_2O \quad (9)$$

The peak in the DTG curve corresponding to the most intense reaction (3) occurs above 400 °C, which has been confirmed in the literature [52]. A slight upward shift to 424 °C in the $Ca(OH)_2$-MC sample suggests the influence of additional compounds, such as residues of pyrolysis gases, on the thermal stability. The peaks representing $Ca(OH)_2$ are much lower in the $Ca(OH)_2$-MC and $Ca(OH)_2$-MC_Cl samples than in the raw calcium hydroxide. This can be explained by the course of the reaction (3) in the bed before the pyrolysis process, where the system was purged

with nitrogen and the bed temperature was 450 °C. The distinct peaks at 664 °C and 704 °C in the $Ca(OH)_2$ samples after pyrolysis as a result of the $CaCO_3$ decomposition reaction [53]:

$$CaCO_3 \rightarrow CaO + CO_2 \quad (10)$$

The total weight loss is the lowest (25.5%) for raw $Ca(OH)_2$, as the process is dominated by dehydroxylation. Higher weight losses (32.7%) for $Ca(OH)_2$-MC and (37.5%) $Ca(OH)_2$-MC_Cl indicate the presence of non–volatile residues deposited during the adsorption of pyrolysis gases. During pyrolysis of the MC_Cl sample gases containing HCl through reaction with $Ca(OH)_2$ (11) or with CaO (12) at 450 °C, the formation of calcium chloride ($CaCl_2$):

$$Ca(OH)_2 + \mathrm{HCl} \rightarrow CaCl_2 + 2H_2O \quad (11)$$

$$CaO + \mathrm{HCl} \rightarrow CaCl_2 + H_2O \quad (12)$$

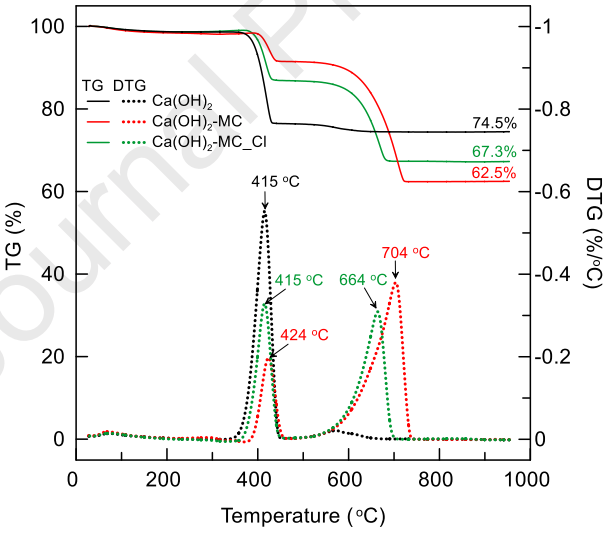

Figure 9. TGA and DTG curves of calcium hydroxide before and after pyrolysis

The resulting $CaCl_2$ is thermally stable and does not decompose within the typical temperature range of the TGA analysis (from room temperature to around 950 °C). Therefore, $CaCl_2$ is formed, and it will not exhibit decomposition peaks in the TGA results. The absence of additional peaks at high temperatures (e.g., above 700 °C) in the TGA and DTG curves suggests that $CaCl_2$ remains in a stable form in the residue after thermal analysis. Practically, the

presence of $CaCl_2$ can reduce the total percentage of weight loss, as it does not decompose during heating. This can be observed in the lower weight loss values for the $Ca(OH)_2$-MC and $Ca(OH)_2$-MC_Cl samples compared to raw of $Ca(OH)_2$. These results highlight the effects of pyrolysis gases, including chlorine, on the decomposition behaviour of $Ca(OH)_2$.

The nitrogen adsorption-desorption isotherms and pore size distributions for sorbent samples are shown in Fig. S2 and Fig. S3 (see supplementary material). According to Fig. S2, the nitrogen adsorption-desorption isotherms demonstrate that adsorption occurs predominantly at higher relative pressures ($p/p_0 > 0.8$), which is characteristic of macroporous materials [54]. The isotherms display a distinct hysteresis loop, a feature typically attributed to capillary condensation occurring within mesopores, confirming the coexistence of macropores and mesopores in the samples. Based on the classification [55], these isotherms exhibit a hybrid Type I–IV shape. The Type I component indicates the presence of micropores that contribute to adsorption at lower relative pressures, whereas the Type IV behaviour reflects mesoporosity with multilayer adsorption and capillary condensation. A comparison between the isotherms of $Ca(OH)_2$-MC and $Ca(OH)_2$-MC_Cl reveals differences in adsorption capacity and isotherm shape. The $Ca(OH)_2$-MC_Cl sample, exhibits a slightly higher adsorption capacity throughout the pressure range. Furthermore, the relative positions and slopes of the adsorption and desorption branches in the hysteresis loops suggest variations in pore size distribution and shape between the samples. The pore size distribution curves showed that pore network was mainly composed of mesopores (2–50 nm) [56] and macropores (50–90 nm). The specific surface area results for the sorbents are shown in Table 5. Unfortunately, the presence of residual water in $Ca(OH)_2$ was a significant factor influencing the result of the Brunauer–Emmett–Teller (BET) analysis. Even after drying at 120 °C for 24 h, chemically bound water or the water adsorbed in the pores of the material was not completely removed, which led to problems with the

484 measurement of adsorption. Negative adsorption values appeared in the isotherm, and pore size
485 analysis was not possible. Therefore, the results for raw $Ca(OH)_2$ are not provided in Table 5.
486 In turn, heating $Ca(OH)_2$-MC in the reactor to 450 °C led to a dehydration reaction. This process
487 likely promoted the development of material porosity through the removal of crystallisation
488 water, resulting in the formation of new pores and the specific surface area was 11.65m^2/g.
489 During pyrolysis, $Ca(OH)_2$-MC acted as both a catalyst and a CO_2 adsorbent, interacting with
490 reactive gases. CO_2 reactions facilitated the formation of calcium carbonate ($CaCO_3$) and
491 contributed to pore opening or enlargement during the process, resulting in an increase in the
492 specific surface area (14.05 m^2/g). Moreover, an increase in the cumulative volume of pores
493 (Barrett-Joyner-Halenda (BJH) method) and a decrease in the average pore diameter were
494 observed in calcium hydroxide after MC_Cl pyrolysis compared to calcium hydroxide after MC
495 pyrolysis. The presence of HCl in the pyrolytic gas stream likely contributed to the increased
496 surface area of $Ca(OH)_2$ compared to conditions without HCl. This effect can be attributed to
497 chemical interactions between HCl and $Ca(OH)_2$, leading to the formation of calcium chloride
498 ($CaCl_2$). These reactions may have altered the surface morphology of the material, created new
499 pores, or enhanced existing ones.

500 Table 5. Specific surface area of applied sorbents

Sample	Surface area analysis (BET), (m^2/g)	Cumulative volume of pores (BJH) adsorption/desorption, (cm^3/g)	Average pore diameter (BJH) ads/des (nm)
$Ca(OH)_2$-MC	11.65	0.0491 / 0.0471	17.68/ 14.73
$Ca(OH)_2$-MC_Cl	14.05	0.0525/ 0.0508	16.10 / 11.72

501 **4. Conclusions**

502 This study demonstrates that pretreatment of maize cob biomass with hydrogen chloride
503 derived from dehydrochlorinated PVC influence on significant structural changes, including

increased porosity and decomposition of hemicellulose, (reduction from 34.3% to 3.7%). The fixed carbon fraction also increased, favouring higher yields of the pyrolysis products. Such compositional adjustments make biomass more reactive, allowing better utilisation during thermal conversion processes.

The application of calcium hydroxide within the pyrolysis reactor emerged as a dual-purpose solution: capture of chlorine and CO_2 while promoting desirable gas–phase reactions. This process resulted in a reduction in CO_2 emissions and a significantly higher hydrogen content in the pyrolysis gas, highlighting its role in improving the environmental performance and energy potential of the system. Moreover, the stabilisation of chlorine within solid products ensures safer bio–oil and char, which can be effectively utilised in various industrial applications.

The innovative use of gaseous hydrogen chloride as a pretreatment agent, sourced from PVC waste, provides an environmentally conscious pathway for biomass upgrading. This method integrates waste management with renewable energy production, addressing critical challenges in both sectors. These findings open new possibilities for enhancing biomass pyrolysis through tailor–made pretreatment strategies and reactor designs aimed at maximising efficiency and minimising environmental footprint.

Acknowledgements

Research project was mainly supported by the program „Excellence initiative – research university" for the AGH University of Krakow [grant AGH No. 501.696.9723]. The investigations concerning impact of chlorine (PVC) was funded by the National Science Centre of Poland [grant No. 2020/39/B/ST8/00883]

References

[1] H. Lee, K. Calvin, D. Dasgupta, G. Krinner, A. Mukherji, P. Thorne, C. Trisos, J.

Romero, P. Aldunce, IPCC Sixth Assessment Report - Synthesis Report, 2023. https://doi.org/10.59327/IPCC/AR6-9789291691647.

[2] S. Sobek, S. Werle, Solar pyrolysis of waste biomass: Part 1 reactor design, Renew. Energy. 143 (2019) 1939–1948. https://doi.org/10.1016/j.renene.2019.06.011.

[3] S. Jha, F. Pattnaik, S. Nanda, O. Zapata, B. Acharya, A.K. Dalai, Investigations of thermal effects during pyrolysis of agro-forestry biomass and physicochemical characterizations of biofuel products, Biocatal. Agric. Biotechnol. 61 (2024) 103379. https://doi.org/10.1016/j.bcab.2024.103379.

[4] R. Muzyka, E. Misztal, J. Hrabak, S.W. Banks, M. Sajdak, Various biomass pyrolysis conditions influence the porosity and pore size distribution of biochar, Energy. 263 (2023) 126128. https://doi.org/10.1016/j.energy.2022.126128.

[5] G. Wang, Y. Dai, H. Yang, Q. Xiong, K. Wang, J. Zhou, Y. Li, S. Wang, A review of recent advances in biomass pyrolysis, Energy and Fuels. 34 (2020) 15557–15578. https://doi.org/10.1021/acs.energyfuels.0c03107.

[6] Y. Wang, J.J. Wu, Thermochemical conversion of biomass: Potential future prospects, Renew. Sustain. Energy Rev. 187 (2023) 113754. https://doi.org/10.1016/j.rser.2023.113754.

[7] C. Quan, Y. Zhou, J. Wang, C. Wu, N. Gao, Biomass-based carbon materials for CO_2 capture: A review, J. CO_2 Util. 68 (2023) 102373. https://doi.org/10.1016/j.jcou.2022.102373.

[8] M. Afraz, F. Muhammad, J. Nisar, A. Shah, S. Munir, G. Ali, A. Ahmad, Production of value added products from biomass waste by pyrolysis: An updated review, Waste Manag. Bull. 1 (2024) 30–40. https://doi.org/10.1016/j.wmb.2023.08.004.

[9] G. Guerriero, J.F. Hausman, J. Strauss, H. Ertan, K.S. Siddiqui, Lignocellulosic biomass: Biosynthesis, degradation, and industrial utilization, Eng. Life Sci. 16 (2016)

554 1–16. https://doi.org/10.1002/elsc.201400196.
555 [10] J. Baruah, B.K. Nath, R. Sharma, S. Kumar, R.C. Deka, D.C. Baruah, E. Kalita, Recent
556 trends in the pretreatment of lignocellulosic biomass for value-added products, Front.
557 Energy Res. 6 (2018) 1–19. https://doi.org/10.3389/fenrg.2018.00141.
558 [11] A.K. Kumar, S. Sharma, Recent updates on different methods of pretreatment of
559 lignocellulosic feedstocks: a review, Bioresour. Bioprocess. 4 (2017) 1–19.
560 https://doi.org/10.1186/s40643-017-0137-9.
561 [12] R.S. Abolore, S. Jaiswal, A.K. Jaiswal, Green and sustainable pretreatment methods for
562 cellulose extraction from lignocellulosic biomass and its applications: A review,
563 Carbohydr. Polym. Technol. Appl. 7 (2024) 100396.
564 https://doi.org/10.1016/j.carpta.2023.100396.
565 [13] D. Chen, D. Gao, S. Huang, S.C. Capareda, X. Liu, Y. Wang, T. Zhang, Y. Liu, W.
566 Niu, Influence of acid-washed pretreatment on the pyrolysis of corn straw: A study on
567 characteristics, kinetics and bio-oil composition, J. Anal. Appl. Pyrolysis. 155 (2021)
568 105027. https://doi.org/10.1016/j.jaap.2021.105027.
569 [14] S. Zhou, Y. Xue, J. Cai, C. Cui, Z. Ni, Z. Zhou, An understanding for improved
570 biomass pyrolysis: Toward a systematic comparison of different acid pretreatments,
571 Chem. Eng. J. 411 (2021) 128513. https://doi.org/10.1016/j.cej.2021.128513.
572 [15] Y. Ren, Z. Wang, J. Chen, H. Gao, K. Guo, X. Wang, X. Wang, Y. Wang, H. Chen, J.
573 Zhu, Y. Zhu, Effect of water/acetic acid washing pretreatment on biomass chemical
574 looping gasification (BCLG) using cost-effective oxygen carrier from iron-rich sludge
575 ash, Energy. 272 (2023) 127161. https://doi.org/10.1016/j.energy.2023.127161.
576 [16] S.R.G. Oudenhoven, A.G.J. van der Ham, H. van den Berg, R.J.M. Westerhof, S.R.A.
577 Kersten, Using pyrolytic acid leaching as a pretreatment step in a biomass fast
578 pyrolysis plant: Process design and economic evaluation, Biomass and Bioenergy. 95

(2016) 388–404. https://doi.org/10.1016/j.biombioe.2016.07.003.

[17] D.O. Usino, T. Sar, P. Ylitervo, T. Richards, Effect of Acid Pretreatment on the Primary Products of Biomass Fast Pyrolysis, Energies. 16 (2023). https://doi.org/10.3390/en16052377.

[18] A.T. Hoang, S. Nizetic, H.C. Ong, C.T. Chong, A.E. Atabani, V.V. Pham, Acid-based lignocellulosic biomass biorefinery for bioenergy production: Advantages, application constraints, and perspectives, J. Environ. Manage. 296 (2021) 113194. https://doi.org/10.1016/j.jenvman.2021.113194.

[19] Y. He, J. Zhang, J. Bao, Dry dilute acid pretreatment by co-currently feeding of corn stover feedstock and dilute acid solution without impregnation, Bioresour. Technol. 158 (2014) 360–364. https://doi.org/10.1016/j.biortech.2014.02.074.

[20] S. Shao, J. Zhang, J. Bao, Reduction of Reactor Corrosion by Eliminating Liquid-Phase Existence in Dry Dilute Acid Pretreatment of Corn Stover, Energy and Fuels. 31 (2017) 6140–6144. https://doi.org/10.1021/acs.energyfuels.7b00446.

[21] S. Shao, Y. Zhang, H. Shen, C. Jin, H. Gu, Z. Qiu, Enhanced bioethanol production from Compositae plant stalks: Integrating dry acid pretreatment and fungal mediated biodetoxification, Sustain. Chem. Pharm. 42 (2024) 101817. https://doi.org/10.1016/j.scp.2024.101817.

[22] H. Gu, X. Han, J. Zhang, J. Bao, Upgrading dry acid pretreatment by post-hydrolysis for carbon efficient conversion of lignocellulose, Bioresour. Technol. 394 (2024) 130261. https://doi.org/10.1016/j.biortech.2023.130261.

[23] C.L. Lin, J.H. Lin, C.L. Pan, Y.H. Chang, Degradation of corn starch with different moisture content by gaseous hydrogen chloride, Int. J. Biol. Macromol. 219 (2022) 463–472. https://doi.org/10.1016/j.ijbiomac.2022.07.218.

[24] T. Lourençon, M. Altgen, T. Pääkkönen, V. Guccini, P. Penttilä, E. Kontturi, L.

Rautkari, Effect of Moisture on Polymer Deconstruction in HCl Gas Hydrolysis of Wood, ACS Omega. 7 (2022) 7074–7083. https://doi.org/10.1021/acsomega.1c06773.

[25] A.T. Kilpinen, K. Nieminen, E. Kontturi, Pretreatment to Retrieve Xylose and Xylooligosaccharides by HCl Gas Directly from Biomass, ACS Sustain. Chem. Eng. 12 (2024) 2135–2138. https://doi.org/10.1021/acssuschemeng.3c07532.

[26] Y. Wang, T. Pääkkönen, K. Miikki, N.H. Maina, K. Nieminen, A. Zitting, P. Penttilä, H. Tao, E. Kontturi, Degradation of cellulose polymorphs into glucose by HCl gas with simultaneous suppression of oxidative discoloration, Carbohydr. Polym. 302 (2023) 120388. https://doi.org/10.1016/j.carbpol.2022.120388.

[27] L. Dostie, K. Rausis, I.M. Power, Passive direct air capture using calcium oxide powder: The importance of water vapor, J. Clean. Prod. 457 (2024) 142394. https://doi.org/10.1016/j.jclepro.2024.142394.

[28] W. Jerzak, I. Kalemba-Rec, A. Magdziarz, Dechlorination of Polyvinyl Chloride and Investigation of its Co-pyrolysis with Maize Cob, in: M. Ban, D.A. Gracia, N. Duić (Eds.), 19th Conf. Sustain. Dev. Energy, Water Environ. Syst. Septempber 8-12, 2024, Rome, 2024: p. 785.

[29] N. Dong, H. Hui, S. Li, L. Du, Study on preparation of aromatic-rich oil by thermal dechlorination and fast pyrolysis of PVC, J. Anal. Appl. Pyrolysis. 169 (2023) 105817. https://doi.org/10.1016/j.jaap.2022.105817.

[30] X. Chen, X. Bai, A single-step upcycling of PVC-containing municipal solid waste compositions for greener chemicals and clean solids as fuel or oil absorbent, J. Energy Inst. 111 (2023) 101405. https://doi.org/10.1016/j.joei.2023.101405.

[31] ISO 18134. Solid biofuels — Determination of moisture content Part 3: Moisture in general analysis sample, (2023) 1–5. https://www.iso.org/standard/83193.html.

[32] ISO 18123. Solid biofuels — Determination of volatile matter, (2023) 1–9.

https://www.iso.org/standard/83192.html.

[33] ISO 18122. Solid biofuels — Determination of ash content, (2022) 1–7. https://www.iso.org/standard/83190.html.

[34] ISO 16948. Solid biofuels — Determination of total content of carbon, hydrogen and nitrogen, (2015) 1–9. https://www.iso.org/standard/58004.html.

[35] ISO 587. Coal and coke — Determination of chlorine using Eschka mixture, (2020) 1–8. https://www.iso.org/standard/79739.html.

[36] ISO 16472. Animal feeding stuffs. Determination of amylase-treated neutral detergent fibre content (aNDF), (2006) 1–16. https://www.iso.org/standard/37898.html.

[37] ISO 13906. Animal feeding stuffs - Determination of acid detergent fibre (ADF) and acid detergent lignin (ADL) contents, (2008) 1–17. https://www.iso.org/standard/43032.html.

[38] I. Langmuir, The adsorption of gases on plane surface of glass, mica and olatinum, J. Am. Chem. Soc. 40 (1918) 1361–1403. https://doi.org/10.1021/ja02242a004.

[39] N. Kuzhiyil, D. Dalluge, X. Bai, K.H. Kim, R.C. Brown, Pyrolytic sugars from cellulosic biomass, ChemSusChem. 5 (2012) 2228–2236. https://doi.org/10.1002/cssc.201200341.

[40] A.A. Vaidya, K.D. Murton, D.A. Smith, G. Dedual, A review on organosolv pretreatment of softwood with a focus on enzymatic hydrolysis of cellulose, Biomass Convers. Biorefinery. 12 (2022) 5427–5442. https://doi.org/10.1007/s13399-022-02373-9.

[41] M. Balajii, S. Niju, Banana peduncle – A green and renewable heterogeneous base catalyst for biodiesel production from Ceiba pentandra oil, Renew. Energy. 146 (2020) 2255–2269. https://doi.org/10.1016/j.renene.2019.08.062.

[42] C. Kundu, S.P. Samudrala, M.A. Kibria, S. Bhattacharya, One-step peracetic acid

pretreatment of hardwood and softwood biomass for platform chemicals production, Sci. Rep. 11 (2021) 1–11. https://doi.org/10.1038/s41598-021-90667-9.

[43] G. Kłosowski, D. Mikulski, Changes in various lignocellulose biomasses structure after microwave-assisted hydrotropic pretreatment, Renew. Energy. 219 (2023). https://doi.org/10.1016/j.renene.2023.119387.

[44] R. Wu, Q. Ye, K. Wu, L. Wang, H. Dai, Highly efficient CO_2 adsorption of corn kernel-derived porous carbon with abundant oxygen functional groups, J. CO_2 Util. 51 (2021) 101620. https://doi.org/10.1016/j.jcou.2021.101620.

[45] S. Li, D. Tasnady, Biochar for Soil Carbon Sequestration: Current Knowledge, Mechanisms, and Future Perspectives, C-Journal Carbon Res. 9 (2023). https://doi.org/10.3390/c9030067.

[46] P.J. White, M.R. Broadley, Chloride in soils and its uptake and movement within the plant: A review, Ann. Bot. 88 (2001) 967–988. https://doi.org/10.1006/anbo.2001.1540.

[47] X. Hu, M. Gholizadeh, Progress of the applications of bio-oil, Renew. Sustain. Energy Rev. 134 (2020) 110124. https://doi.org/10.1016/j.rser.2020.110124.

[48] S. Singh, K.K. Pant, M. Krishania, Current perspective for bio-oil production from agricultural residues in commercialization aspect: A review, J. Anal. Appl. Pyrolysis. 175 (2023) 106160. https://doi.org/10.1016/j.jaap.2023.106160.

[49] Q. Wang, X. Zhang, S. Sun, Z. Wang, D. Cui, Effect of CaO on Pyrolysis Products and Reaction Mechanisms of a Corn Stover, ACS Omega. 5 (2020) 10276–10287. https://doi.org/10.1021/acsomega.9b03945.

[50] C.F. Magoua Mbeugang, B. Li, D. Lin, X. Xie, S. Wang, S. Wang, S. Zhang, Y. Huang, D. Liu, Q. Wang, Hydrogen rich syngas production from sorption enhanced gasification of cellulose in the presence of calcium oxide, Energy. 228 (2021) 120659.

https://doi.org/10.1016/j.energy.2021.120659.

[51] Y. Tang, J. Dong, Y. Zhao, G. Li, Y. Chi, E. Weiss-Hortala, A. Nzihou, G. Luo, C. Ye, Hydrogen-Rich and Clean Fuel Gas Production from Co-pyrolysis of Biomass and Plastic Blends with CaO Additive, ACS Omega. 7 (2022) 36468–36478. https://doi.org/10.1021/acsomega.2c04279.

[52] J. Yan, C.Y. Zhao, Thermodynamic and kinetic study of the dehydration process of $CaO/Ca(OH)_2$ thermochemical heat storage system with Li doping, Chem. Eng. Sci. 138 (2015) 86–92. https://doi.org/10.1016/j.ces.2015.07.053.

[53] W. Jerzak, P. Murzyn, M. Kuźnia, A. Magiera, Trace elements retention in bottom ashes during coal combustion with hydrated lime additions, Energy Sources, Part A Recover. Util. Environ. Eff. (2019). https://doi.org/10.1080/15567036.2019.1636157.

[54] H. Laksaci, A. Khelifi, M. Trari, A. Addoun, Synthesis and characterization of microporous activated carbon from coffee grounds using potassium hydroxides, J. Clean. Prod. 147 (2017) 254–262. https://doi.org/10.1016/j.jclepro.2017.01.102.

[55] S. Brunauer, L.S. Deming, W.E. Deming, E. Teller, On a Theory of the van der Waals Adsorption of Gases, J. Am. Chem. Soc. 62 (1940) 1723–1732. https://doi.org/10.1021/ja01864a025.

[56] X.Y. Yang, L.H. Chen, Y. Li, J.C. Rooke, C. Sanchez, B.L. Su, Hierarchically porous materials: Synthesis strategies and structure design, Chem. Soc. Rev. 46 (2017) 481–558. https://doi.org/10.1039/c6cs00829a.

Declaration of interests

☒ The authors declare that they have no known competing financial interests or personal relationships that could have appeared to influence the work reported in this paper.

☐ The authors declare the following financial interests/personal relationships which may be considered as potential competing interests: